Control of coherent acoustic phonon generation with external bias in InGaN/GaN multiple quantum wells

C. S. Kim,[1] J. H. Kim,[1] H. Jeong,[2] Y. D. Jho,[2,a)] H. K. Kwon,[3] H. S. Lee,[4] J. S. Park,[4] K. Song,[5] S. H. Kim,[1,6] Y. J. Kim,[5,6] D. Lee,[1] and K. J. Yee[1,6,b)]
[1]*Department of Physics, Chungnam National University, Daejeon 305-764, South Korea*
[2]*Department of Information and Communications, Gwangju Institute of Science and Technology, Gwangju 500-712, South Korea*
[3]*Advanced Technology Laboratory, LG Innotek, Seoul 137-724, South Korea*
[4]*Epivalley, Gyeonggido 433-270, South Korea*
[5]*Korea Basic Science Institute, Daejeon 305-333, South Korea*
[6]*Graduate School of Analytical Science and Technology, Chungnam National University, Daejeon 305-764, South Korea*

(Received 11 January 2012; accepted 17 February 2012; published online 6 March 2012)

Control of acoustic phonon generation with external bias is demonstrated for an InGaN light-emitting diode by performing femtosecond pump–probe measurements. The evolution of both the carrier dynamics and the acoustic phonon strength with an external bias reveals that the acoustic wave is generated during the carrier sweeping process of the depletion field, where electric field screening accompanies stress of the lattice for a piezoelectric material. © *2012 American Institute of Physics*. [http://dx.doi.org/10.1063/1.3692594]

The control of acoustic phonon generation is in high demand for applications using picosecond or femtosecond strain pulses, such as the phonon laser, terahertz radiation source, and nanostructure interface imaging.[1–4] In InGaN/GaN heterostructures, the coherent acoustic phonon has been demonstrated to form through piezoelectric electron–phonon interactions, where photoexcitation itself drives local lattice deformations.[5–8]

In the case of InGaN/GaN multiple quantum wells (MQWs), there are polarization fields in the quantum wells that oppose the polarization fields in the barriers, with the direction being determined by whether the strain is compressive or tensile.[9] If strain accompanies the polarization field in a piezoelectric material, the additional electric field will induce stress in the lattice as a counteraction. With regard to optical phonons, ultrafast field screening of the depletion region, which depends on the doping concentration and external bias, has been demonstrated to be the generation mechanism for coherent longitudinal-optical phonon oscillations in GaAs.[10,11] Having high piezoelectricity and good thermomechanical stability, GaN-based material is a good candidate material for testing conversion from mechanical strain to electric field and vice versa. For example, Lin *et al*. reported efficient acoustic pulse generation through the field screening of carriers in the depletion region of a p-n junction.[12] In p-n or p-i-n diode structures, the depletion field is modified by applying an external bias, which affects the carrier drift and the driving force for the coherent acoustic phonon. Since the strain wave propagates at sound velocity, the spatial shape of the strain pulse must depend on the temporal profile of the driving force, which can also be modified by external bias.

In this paper, we report on the control of the acoustic phonon amplitude through the application of electric bias in an InGaN light-emitting diode (LED). The bias dependence of acoustic phonon generation is explained by the dynamic electric field screening of carriers, where the effective barrier and type-II absorption probability are key parameters.

We performed pump–probe measurements in reflection geometry on an InGaN LED having electroluminescence near 405 nm. The active region of the LED consisted of six periods of a 2-nm-thick InGaN quantum well with 10% In composition and an 8-nm-thick GaN barrier, and it was sandwiched between p-doped regions of GaN/AlGaN and n-doped GaN grown by metalorganic chemical vapor deposition on a sapphire substrate. The intrinsic electric field without external bias amounted to a voltage drop of about 3 V between the n-doped and p-doped regions. The band diagram and electric field in the active region were modified by applying external bias voltage ranging from −10 to 3 V.

For photoexcitation of carriers in InGaN quantum wells, femtosecond pulses with a central wavelength of 385 nm (3.22 eV) and pulse duration of 250 fs were obtained by frequency doubling near-infrared pulses from a Ti:sapphire laser. A beam splitter split the pulses into a pump beam with intensity of $\sim 20\,\mu J/cm^2$ and a weaker probe beam. The pump pulse induces transient carriers and subsequent strain generation mostly within the active region. By measuring the reflectivity of a probe pulse with varying time delay between the pump and probe pulses, carrier dynamics and strain wave propagation were studied. We employed the conventional chopping and lock-in amplifier technique to measure sinusoidal strain-induced reflectivity modulations with time delay between pump and probe pulses.

Figure 1(a) shows reflectivity changes as a function of time delay for several external biases, displayed with offsets for clarity. The pump–probe signals can be decomposed into two contributions. One is the overall reflectivity change due

a)Electronic mail: jho@gist.ac.kr.
b)Electronic mail: kyee@cnu.ac.kr.

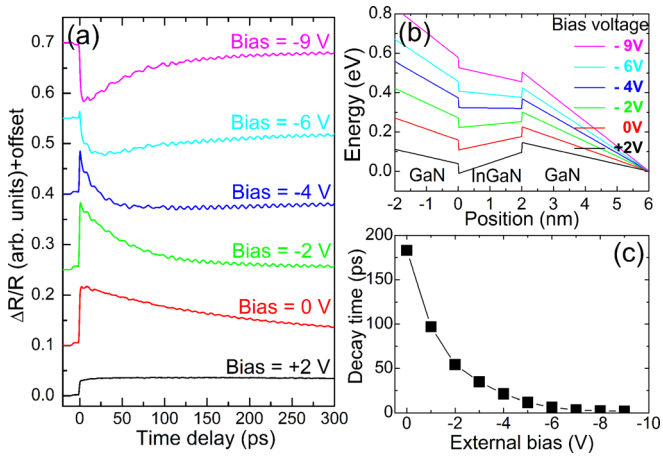

FIG. 1. (Color online) (a) Transient reflection changes for an InGaN LED as a function of the time delay between pump and probe pulses for several external biases. The excitation wavelength was 385 nm. (b) Simulated conduction-band diagram for external biases. (c) Decay time obtained by exponentially fitting the temporal region where the reflectivity decreases.

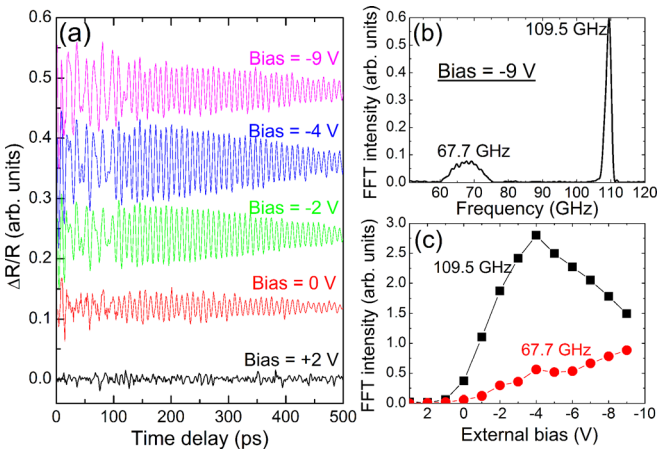

FIG. 2. (Color online) (a) Temporal reflection modulations by acoustic phonons for several measured bias voltages and a wavelength of 385 nm. (b) Fourier transform spectrum of the acoustic phonon oscillations for bias voltage of −9 V. (c) Integrated FFT intensity of the signal at 109.5 GHz and that at 67.7 GHz as functions of the external bias.

to photoexcited carriers, and the other is small sinusoidal modulations with a period of the order of 10 ps. The overall reflectivity dynamics must originate from the pump-induced changes in carrier density and polarization fields.[13]

With there being a relatively strong piezoelectric effect, the electrons and holes excited inside each quantum well will be forced to move in opposite directions under the piezoelectric field, which will induce transient electric fields in each quantum well. The in-well screening will decrease as the excited carriers disappear through transport or electron–hole recombination. As can be understood from the simulated band diagrams in Fig. 1(b), at low bias voltage, the electric field within each quantum well is in the opposite direction to the macroscopic electric field throughout the active region. Screening of the in-well electric field will occur instantaneously with the generation of photoexcited carriers in quantum wells. If the carriers are transported through the tunneling, the in-well screening and the non-equilibrium carrier density in quantum wells will disappear, and the macroscopic field screening will induce additional opposite fields. We propose that the initial positive reflectivity change originates from the contribution of the in-well screening and the carriers excited in quantum wells, while the reflectivity change becomes negative at high reverse bias through the increased contribution of the macroscopic field screening.

As the effective barrier is reduced by the reverse bias as in Fig. 1(b), the movement of the electrons and holes towards the n-doped region and p-doped region, respectively, will accelerate.[14] As shown in Fig. 1(a), the change in reflectivity decreases almost instantaneously for reverse biases of −6 and −9 V. The decay rate in Fig. 1(c), which was obtained by exponentially fitting the temporal region within which the reflectivity decreases, is qualitatively consistent with the expected carrier tunneling time.[14]

The sinusoidal modulation of the reflectivity strongly depends on the external bias. Figure 2(a) shows the oscillatory parts extracted from the pump-probe signals for several external biases. A pump pulse generates a strain wave, and the oscillatory signal is known to originate from the Fabry–Perot interference between probe photons reflected at the surface and those reflected at the strain wave.[15,16] As the strain wave propagates with a time delay, constructive and destructive interference alternate to produce the oscillatory acoustic phonon signal in time-resolved reflectivity.

It is interesting that the acoustic phonons are almost completely suppressed at forward bias of +2 V, even though the carrier density excited in quantum wells does not depend considerably on external bias. The strong dependence of the acoustic phonon generation on external bias as in Fig. 2(a) cannot be explained by the general piezoelectric electron–phonon interactions, where the driving force is a strict function of the carrier density.[5] Our results, on the contrary, suggest that the dominant generation mechanism is the piezoelectric force, accompanied by the field screening of photoexcited carriers. Although the photon energy is lower than the band gap of the GaN barrier, carriers can be excited at GaN barriers through type-II transition where the transition probability is considerable at high reverse bias.[17] The carrier density excited in quantum wells by type-I transition must be much larger than that in barriers, but the screening efficiency may be low because the well width is less than the bulk exciton Bohr radius (∼3.4 nm), with the electron wavefunction confined in the well. On the other hand, the carriers excited at barriers can efficiently screen the piezoelectric field. The screening speed in the barrier and the type-II transition coefficient increases with the reverse bias.[17] Thus, the small amplitude at forward or low reverse bias can be explained by the negligible type-II carrier excitation at barriers and the inefficient screening within wells. As the reverse bias increases, the barrier screening becomes prominent as is revealed by the stronger acoustic phonon amplitude in Fig. 2(a).

Figure 2(b) shows the fast Fourier transformation (FFT) spectrum of the time domain oscillations at a bias of −9 V. The signal at 109.5 GHz corresponds to the propagating strain wave, where the frequency (ν_{AC}) is related to the sound velocity (C_s), refractive index (n), and probe wavelength (λ) such that $\nu_{AC} = 2C_s\, n/\lambda$. With n = 2.56, the propagation speed is determined as 8230 m/s, which agrees well with values reported for GaN-based materials. In addition to

the mode at 109.5 GHz, there is a rather broad signal at 67.7 GHz, which will be described later.

Figure 2(c) shows the FFT intensity as a function of the external bias for both the signal at 109.5 GHz and that at 67.7 GHz. The intensity is negligible at forward biases higher than +1 V and increases with reverse bias until −4 V. The intensity at 109.5 GHz decreases for reverse bias larger than −4 V, while the signal at 67.7 GHz increases consistently up to −9 V. For the strain wave to form its shape efficiently, the driving force is required to last for half of the phonon period. It is possible that the tunneling and carrier depletion occur too quickly at high reverse bias such that the strain generation is degraded.

Depending on whether the time delay is more or less than 120 ps, there are obvious differences in the oscillatory behaviors in Fig. 2(a). This kind of abrupt signal change at a specific time delay with the strain propagation has been interpreted as being due to impedance mismatch at the hetero-interface or at the interface between different doping regions.[18,19] To specify the origin of the temporal border more clearly, we performed sliding-window FFT (SWFFT) for the temporal oscillations at bias of −9 V. Figure 3(a) is a contour plot of the SWFFT spectrum as a function of the time delay on the horizontal axis and of frequency on the vertical axis. Figure 3(b) shows the FFT intensity as a function of time delay for each peak. Figures 3(a) and 3(b) clearly show that the signal at 67.7 GHz is predominantly earlier than 120 ps, and the signal at 109.5 GHz strengthens as the 67.7 GHz signal weakens near 120 ps.

The transmission electron microscopy (TEM) image of the sample in Fig. 3(c) clearly displays each interface of the layers, enabling a good estimate of the individual-layer thicknesses. A portion of the strain wave generated in the InGaN/GaN MQW region will propagate towards the surface and will then be reflected with a π phase shift.[20,21] Taking the strain propagation speed determined from the signal

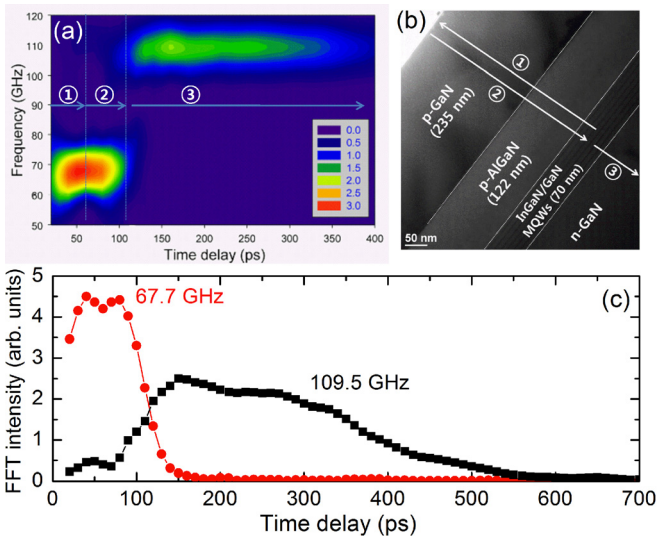

FIG. 3. (Color online) (a) Contour plot of the SWFFT intensity at bias of −9 V as a function of the time delay (horizontal axis) and frequency (vertical axis). (b) High-resolution TEM image showing the device structure. The white arrows indicate the proposed sequential movement of the strain wave excited in the MQW region, corresponding with the temporal segment of the SWFFT signal in Fig. 3(a). (c) Temporal evolution of the FFT signal at 67.7 GHz and that at 109.5 GHz as functions of the time delay.

frequency of 67.7 GHz into account, time interval (1) in the contour plot with time delay $t < 60$ ps corresponds roughly to the temporal window when the strain transits from the MQW to the surface, and interval (2) of $60 < t < 120$ ps corresponds to when the reflected strain propagates back to the MQW, and the wave moves into the n-doped region at a time delay of later than 120 ps. Although the origin of the 67.7 GHz signal is not obvious at this moment, we find that the signal prevails when the strain wave propagates in the p-doped region of the GaN or AlGaN in our LED structure.

In conclusion, we demonstrated that the amplitude of coherent acoustic phonons can be controlled by external biases in an InGaN MQW LED structure. The acoustic wave generation mechanism is dominated by the ultrafast electric-field screening of the piezoelectric field at barriers, where the barrier excitation by type-II absorption strongly depends on the applied bias. Comparison of the layer structure and the temporal evolution of the signal reveals that the acoustic phonon frequency is 67.7 GHz when the strain wave propagates in the p-doped region.

This work was supported by National Research Foundation of Korea Grants funded by the Korean Government (Basic Science Research Program: 2009-0085432 and 2009-0090559 and 2009 University–Institute Cooperation Program, SRC: 2010-0001859). Y.D.J. acknowledges support from the Fusion-Tech. Developments for THz Info. & Comm. Program of GIST in 2010.

[1]A. Huynh, N. D. Lanzillotti-Kimura, B. Jusserand, B. Perrin, A. Fainstein, M. F. Pascual-Winter, E. Peronne, and A. Lemaitre, Phys. Rev. Lett. **97**, 115502 (2006).
[2]R. P. Beardsley, A. V. Akimov, M. Henini, and A. J. Kent, Phys. Rev. Lett. **104**, 085501 (2010).
[3]M. R. Armstrong, E. J. Rees, K. Y. Kim, J. H. Glownia, W. M. Howard, E. L. Piner, and J. C. Roberts, Nature Phys. **5**, 285 (2009).
[4]B. C. Daly, N. C. Holme, T. Buma, C. Branciard, T. B. Norris, D. M. Tennant, J. A. Taylor, J. E. Bower, and S. Pau, Appl. Phys. Lett. **84**, 5180 (2004).
[5]C. K. Sun, J. C. Liang, C. J. Stanton, A. Abare, L. Coldren, and S. P. DenBaars, Appl. Phys. Lett. **75**, 1249 (1999).
[6]U. Ozgur, C. W. Lee, and H. O. Everitt, Phys. Rev. Lett. **86**, 5604 (2001).
[7]J. S. Yahng, Y. D. Jho, K. J. Yee, E. Oh, J. C. Woo, D. S. Kim, G. D. Sanders, and C. J. Stanton, Appl. Phys. Lett. **80**, 4723 (2002).
[8]G. D. Sanders and C. J. Stanton, Phys. Rev. B **74**, 205303 (2006).
[9]G. Martin, A. Botchkarev, A. Rockett, and H. Morkoç, Appl. Phys. Lett. **68**, 2541 (1996).
[10]T. Pfeifer, T. Dekorsy, W. Kütt, and H. Kurz, Appl. Phys. A **55**, 482 (1992).
[11]T. Dekorsy, T. Pfeifer, W. Kütt, and H. Kurz, Phys. Rev. B **47**, 3842 (1993).
[12]K. H. Lin, C. T. Yu, Y. C. Wen, and C. K. Sun, Appl. Phys. Lett. **86**, 093110 (2005).
[13]X.-C. Long, R. A. Myers, S. R. J. Brueck, R. Ramer, K. Zheng, and S. D. Hersee, Appl. Phys. Lett. **67**, 1349 (1995).
[14]Y. D. Jho, J. S. Yahng, E. Oh, and D. S. Kim, Appl. Phys. Lett. **79**, 1130 (2001).
[15]C. Thomsen, H. T. Grahn, M. H. Maris, and J. Tauc, Phys. Rev. B **34**, 4129 (1986).
[16]R. Liu, G. D. Sanders, C. J. Stanton, C. S. Kim, J. S. Yahng, Y. D. Jho, K. J. Yee, E. Oh, and D. S. Kim, Phys. Rev. B **72**, 195335 (2005).
[17]C. S. Kim, J. H. Kim, K. J. Yee, H. K. Kwon, H. S. Lee, and J. S. Park, J. Korean Phys. Soc. **57**, 793 (2010).
[18]K. Mizoguchi, M. Hase, S. Nakashima, and M. Nakayama, Phys. Rev. **60**, 8262 (1999).
[19]F. Hudert, A. Bartels, T. Dekorsy, and K. Köhler, J. Appl. Phys. **104**, 123509 (2008).
[20]H. T. Grahn, H. J. Maris, and J. Tauc, IEEE J. Quantum Electron. **25**, 2562 (1989).
[21]P. A. Mante, A. Devos, and A. Le Louarn, Phys. Rev. B **81**, 113305 (2010).